

Mode matching in second order susceptibility metamaterials

Sébastien Héron,^{1,2} Patrick Bouchon,^{1,*} and Riad Haïdar^{1,3}

¹*MINAO - ONERA, The French Aerospace Lab, 91761 Palaiseau, France*

²*MINAO - Laboratoire de Photonique et de Nanostructures (LPN-CNRS), Université Paris-Saclay, Route de Nozay, 91460 Marcoussis, France*

³*École Polytechnique, Département de Physique, Université Paris-Saclay, 91128 Palaiseau, France*
(Dated: June 30, 2021)

We present an effective model for a subwavelength periodically patterned metallic layer, its cavities being filled with a nonlinear dielectric material, which accounts for both the linear and second order behavior. The effective non linear susceptibility for the homogenized layer is driven by the nonlinearity of the dielectric material and by the geometrical parameters, thus leading to much higher susceptibility than existing materials. This leads to a huge enhancement of non linear processes when used together with resonances. Furthermore, multiple resonances are taking place in the metallic cavities, and we investigate the mode matching situations for frequency conversion processes and show how it enhances further their efficiency.

PACS numbers: 42.65.-k, 42.65.Ky, 78.67.Pt

Metamaterials are artificial materials, obtained with subwavelength patterned elements, that exhibit effective electromagnetic properties which depend not only on the material, but also on the geometry. They have given birth to original and unprecedented behaviors both in the linear and non linear regime, such as optical cloaking, phase matched negative index or left-handed metamaterials [1–3]. Subwavelength patterned elements can behave as nanoantennas able to funnel the incoming light and concentrate it in a small volume, which is extremely appealing in the context of non linear optics [4–8]. Indeed, optical nanoantennas can provide huge enhancement of the electric field, and even if the volume at stake is smaller compared to the whole device, nonlinear effects can be boosted. Most of the nanoantennas reported in the literature are metallic, as they can confine the field more easily than dielectric antenna. So the surface nonlinearities of the metal itself are enhanced [5, 9–11], even if dielectric materials can provide much higher volume nonlinearities.

Besides, there are two important stakes when considering a non linear metamaterial. The first is to predict the linear and non linear properties of the patterned material by its geometrical parameters. It can be done for instance with the Maxwell Garnett formalism [12], through field averaging [13] or by retrieving it from rigorous computations or experiments [14]. The second stake consists in finding metamaterials exhibiting multiple resonances so as to enhance the field at each one of the wavelength involved in the frequency conversion process. Lately, several metallic mode matching nanostructures have been suggested to further improve the efficiency of non linear effects either based on plasmonic nanoantennas [15, 16] or on phased-array sources [17].

In this letter, we report on mode matching in a high susceptibility metamaterial for frequency conversion. The investigated structure consists in a patterned

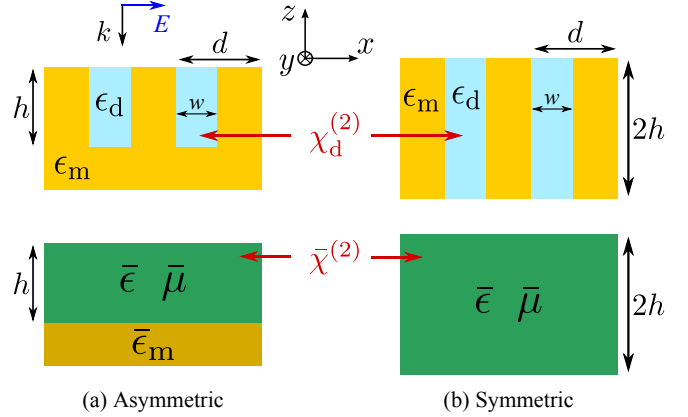


FIG. 1. (a) Periodic grating (period d) of metallic grooves of width w and height h , filled with a non linear dielectric (permittivity ϵ_d , non linear susceptibility $\chi_d^{(2)}$.) The waves are normally incident and TM polarized with wave vectors \mathbf{k} lying in the xOz plane. Below is shown the equivalent metamaterial, that consists in an homogeneous layer with effective permittivity, permeability and non linear susceptibility. (b) Periodic grating of metallic slits filled with a non linear dielectric, which parameters are similar to the reflecting case.

metallic layer, filled with a non linear dielectric, that melts the high confinement properties of metallic nanoantennas and the high non linear susceptibility of chosen dielectric materials. It additionally exhibits multiple Fabry-Perot resonances that can be used for mode matching. First, we present an effective model that fairly accounts for both linear and non linear behaviors of the structure. Its effective linear and non linear optical properties are mainly determined by the aperture ratio. One of the main differences with previously studied plasmonic structures lies in the monitoring of the non linear response by the material filling the holes in the metallic layer rather than the metallic surface generation itself. Then, we show how mode matching can be achieved in

the case of second harmonic generation (SHG) and difference frequency generation (DFG), allowing to reach higher conversion efficiency. These results are scalable to large spectral ranges, and can be adapted in the context of metasurfaces based on MIM antennas.

We aim at describing a subwavelength periodic metal-dielectric layer as an effective medium where the dielectric inclusions display a second order non linear susceptibility. Two configurations of this layer are considered, as shown in Fig. 1. In the one case, the metal-dielectric layer is placed upon a metallic substrate (grating of grooves) and acts as a reflection device and in the other case, the metal-dielectric layer is surrounded by air (grating of slits). For the sake of simplicity, the permittivity of the metal ϵ_m is considered identical in the layer and the substrate, while the dielectric inclusions bear a permittivity ϵ_d and a non linear susceptibility tensor $\chi_d^{(2)}$ which contains only $\chi_{iii}^{(2)}$ terms. The incoming wave is normally incident and transverse magnetic (TM) polarized, at the wavelength λ with a wave vector $k_0 = 2\pi/\lambda$. The period of the system is d and is subwavelength, the grooves or slits have a height h and a width w . The transmission case (Fig. 1 (b)) has previously been described as a metamaterial for perfect metals and was involving an effective thickness [18, 19]. One of the first challenge is to take a lossy metal into account, and to describe the effective layer through the sole effective optical properties $\bar{\epsilon}$, $\bar{\mu}$ and $\bar{\chi}^{(2)}$.

First, the normalized wave vector of the fundamental mode $\sqrt{\epsilon_{\text{TM}}}$ propagating in the plane waveguide set by the two metallic surfaces obeys to the equation:

$$\tanh\left(\sqrt{\epsilon_{\text{TM}} - \epsilon_d} \frac{w}{2}\right) = -\frac{\epsilon_d}{\epsilon_m} \sqrt{\frac{\epsilon_{\text{TM}} - \epsilon_m}{\epsilon_{\text{TM}} - \epsilon_d}}. \quad (1)$$

After some tedious calculations, this equation can be solved at the first order since $\epsilon_d \ll \epsilon_m$, and is written as:

$$\epsilon_{\text{TM}} = \epsilon_d \left(1 + \frac{2\delta}{w} - \frac{\epsilon_d}{\epsilon_m}\right), \quad (2)$$

where $\delta = i\lambda/2\pi\sqrt{\epsilon_m}$ is the metal skin depth.

The light incoming onto the structure is either reflected or funneled into the slit [20, 21], so that the energy in the metal-dielectric layer is contained in the dielectric inclusions. Consequently, the stored energy is the same in both the effective layer and in the dielectric inclusions:

$$\int_{z=0}^{z=h} \int_{x=0}^{x=d} \mathbf{E} \cdot \bar{\mathbf{D}} = \int_{z=0}^{z=h} \int_{x=0}^{x=w} \mathbf{E} \cdot \mathbf{D}, \quad (3)$$

where \mathbf{D} is the electric displacement field, and $\bar{\mathbf{E}}$ and $\bar{\mathbf{D}}$ stand for the fields value in the effective layer. It must be emphasized that the bounds of integration along x have been limited to the dielectric since the energy stored in the metallic sidewalls is negligible. Indeed, at

the metal-dielectric interface normal to the x axis, the x component of the electric field is discontinuous, and the normal electric field on each side are linked by:

$$\frac{E_x(x = w^-)}{E_x(x = w^+)} = \frac{\epsilon_m}{\epsilon_d} \gg 1. \quad (4)$$

Thus, the amplitude of the electric fields inside the dielectric inclusion is far greater than inside the metal.

We consider that the fundamental guided mode is phase and amplitude invariant along the x direction, so that Eq. 3 is expressed as:

$$d \times \int_{z=0}^{z=h} \bar{\epsilon} \bar{E}^2 = w \times \int_{z=0}^{z=h} \epsilon_d E^2. \quad (5)$$

Besides, this equation is valid for all h , so it can be further simplified to $\bar{E}^2 d \bar{\epsilon} = E^2 w \epsilon_d$. The potential difference inside one period, has to be equal between the original configuration and the effective one, so that $\bar{E}d = Ew$. The effective permittivity is then obtained as:

$$\bar{\epsilon} = \epsilon_d \times \frac{d}{w}. \quad (6)$$

Eventually, the phase accumulated by a wave during its propagation through the structure is the same in both cases, $kh = \bar{k}h$. It writes as $\bar{\epsilon}\bar{\mu} = \epsilon_{\text{TM}}$ where the effective layer is chosen magnetic, and its effective permeability can be expressed thanks to Eq. 6:

$$\bar{\mu} = \frac{\epsilon_{\text{TM}}}{\epsilon_d} \times \frac{w}{d}. \quad (7)$$

In the asymmetric case (see Fig. 1(b)), the equivalent layer has to be deposited on a mirror which displays an effective permittivity $\bar{\epsilon}_m$ different from the one of the metal. It can be expressed by matching the reflection coefficients at the bottom of the slit:

$$\frac{\sqrt{\bar{\epsilon}/\bar{\mu}} - \sqrt{\bar{\epsilon}_m}}{\sqrt{\bar{\epsilon}/\bar{\mu}} + \sqrt{\bar{\epsilon}_m}} = \frac{\sqrt{\epsilon_{\text{TM}}} - \sqrt{\epsilon_m}}{\sqrt{\epsilon_{\text{TM}}} + \sqrt{\epsilon_m}}. \quad (8)$$

The effective permittivity of the metallic substrate is given by $\bar{\epsilon}_m = \epsilon_m/\bar{\mu}^2$.

In the following, the asymmetric resonator has a period $d = 1 \mu\text{m}$, a width $w = 0,1 \mu\text{m}$ and a height $h = 0,5 \mu\text{m}$. The metal is gold, described by a Drude model fitting Palik data [22] and the dielectric is gallium arsenide which optical properties are taken from the literature [23]. All the parameters are identical for the symmetric case apart for the height $h = 1 \mu\text{m}$. The computations are performed with the B-spline modal method, which makes a fast and exact resolution of Maxwell equations, and can also solve the nonlinear behavior under the undepleted pump approximation [24, 25].

The linear response of both structures shows (see Supplemental Materials [26]) a rather fair agreement obtained with the effective metamaterial. As expected,

these layers induce Fabry-Perot resonances leading to reflectivity dips and transmittivity peaks, at wavelengths determined by solving the phase condition inside the effective layer:

$$\lambda_m = \frac{2\sqrt{\epsilon_{\text{TM}}}h^*}{m - \phi/2\pi}, \quad (9)$$

where $m \in \mathbb{N}^*$, and ϕ is the phase of the bottom reflection coefficient. It is equal to zero for the symmetric situation and to π for the asymmetric one. To take into account the penetration of the propagating mode in the bottom metal in the asymmetric case, an equivalent height $h^* = h + \delta$ is introduced in the asymmetric case and $h^* = h$ in the symmetric one. Streamlines of the Poynting vector at the resonance wavelengths are also shown in Supp. Mat. [26] to illustrate the funneling phenomenon, that was used in Eq. 3.

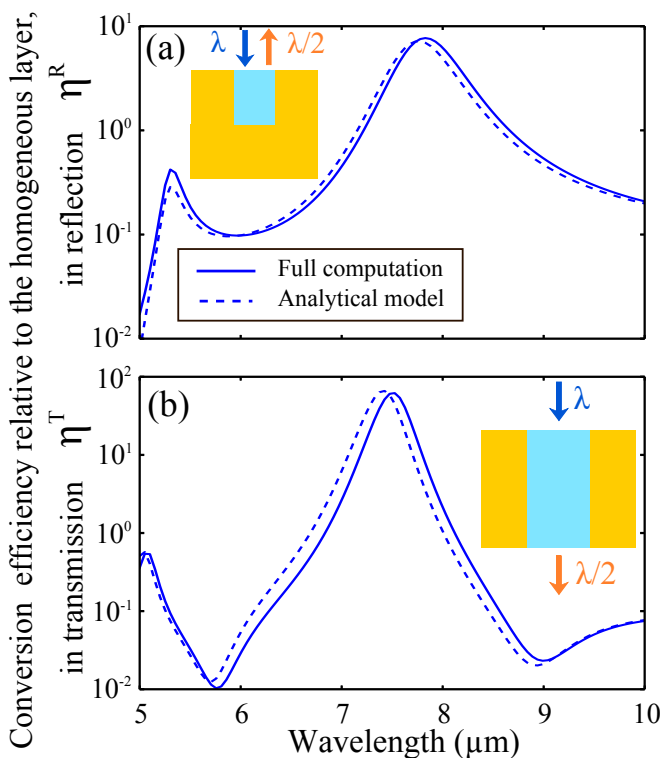


FIG. 2. SHG intensity ratio between structured and unstructured layers: (a) in reflection for the asymmetric case and (b) in transmission for the symmetric one, as a function of the wavelength. Continuous lines stand for the full computation, whereas dashed ones stand for the analytical model. Involved parameters are: $d = 1 \mu\text{m}$, $w = 0,2 \mu\text{m}$, $h = 0,5 \mu\text{m}$ for asymmetric case or $h = 1 \mu\text{m}$ for symmetric case, $\chi^{(2)} = 150 \text{ pm/V}$.

Up to this point, the linear characteristics of the effective layer have been fully determined, but this layer also behaves as a medium with a higher non linear susceptibility. In order to determine its effective value, we state that the nonlinear part of the electromagnetic energy stored in one period is the same in the two cases, as

it was written in Eq. 3 for the linear part of the stored energy. This term is proportional to $\mathbf{E} \cdot \mathbf{P}^{(2)}$, and using the same arguments for integration than before, it leads to:

$$\bar{\chi}^{(2)} \bar{E}_{\lambda_1} \bar{E}_{\lambda_2} \bar{E}_{\lambda_3} \times d = \chi_d^{(2)} E_{\lambda_1} E_{\lambda_2} E_{\lambda_3} \times w, \quad (10)$$

where λ_1 and λ_2 are the pumps wavelengths, and λ_3 the signal wavelength.

The effective nonlinear susceptibility is eventually found to be:

$$\frac{\bar{\chi}^{(2)}}{\chi_d^{(2)}} = \left(\frac{d}{w}\right)^2 \quad (11)$$

It illustrates the great enhancement of the quantity of nonlinear sources inside the cavity of such structures, as d/w is higher than one. For instance, in the two examples of Fig. 2, the effective non linear susceptibility is increased by two orders of magnitude. However, the non linear susceptibility is not the only parameter involved in the efficiency of frequency conversion processes. In fact, due to the high value of the effective permittivity, for most of the wavelengths there is no impedance matching. So the incoming wave is not penetrating the non linear metamaterial, which results in a poor efficiency of the non linear processes.

The efficiency of the second harmonic generation is computed for both structures in Fig. 2. For the sake of comparison, the plotted efficiency is normalized by the intensity of a non patterned gallium arsenide layer, which thickness is chosen so as to display Fabry Perot resonances at the same wavelengths. Following Eqs. (2,9), the equivalent GaAs layer is a bit thicker than the patterned layer. The relative conversion efficiency in reflection as $\eta^R = \frac{I_{\text{out}}^R}{I_{\text{out,ref}}^R}$ where I_{out}^R is the output reflected nonlinear intensity of the metamaterial, and $I_{\text{out,ref}}^R$ is the reflected non linear intensity for an homogeneous layer of gallium arsenide exhibiting a fundamental Fabry Perot resonance at the same wavelength than the metamaterial layer (see Eq. 9). Due to the Eq. 2, the gallium arsenide layer is slightly thicker than the metamaterial layer. The relative conversion efficiency in transmission η^T is defined in a similar way. The GaAs nonlinear susceptibility is chosen as $\chi^{(2)} = 150 \text{ V/pm}$. The full computation for the patterned layer is plotted in continuous lines, while dashed ones stand for the metamaterial model.

Two noticeable behaviors corresponding to resonant and non-resonant cases appear. First, the maximum of the second harmonic signal is indeed one order of magnitude greater leading to interesting resonant values of the enhancement. Second, the ratio drops below 1 meaning that non-resonant behavior gives worse results for the structured resonators. This stems from the small value of the transmission coefficients at the interface in

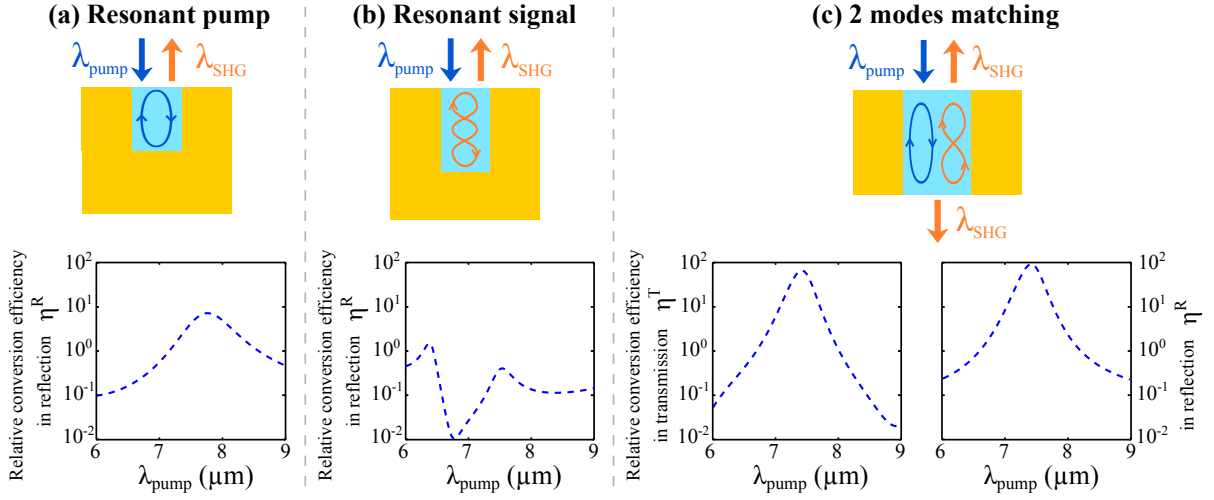


FIG. 3. Three scenarii of resonant behaviours for SHG in the metal-dielectric layer: (a) resonant pump ($h = 0,5 \mu\text{m}$, $h_{\text{GaAs}} = 0,55 \mu\text{m}$) or (b) resonant signal ($h = 0,73 \mu\text{m}$, $h_{\text{GaAs}} = 0,82 \mu\text{m}$) in an asymmetric resonator, and (c) both resonant pump and signal ($h = 1 \mu\text{m}$, $h_{\text{GaAs}} = 1,15 \mu\text{m}$) in a symmetric resonator creating a mode matching configuration. The efficiency curves are shown below as functions of the pump wavelength. In the three cases, $d = 1 \mu\text{m}$ and $w = 0,2 \mu\text{m}$.

the structured case as the impedance $Z = \sqrt{\mu/\epsilon}$ reaches huge values in this case. The second harmonic light is hardly driven to the outer medium compared to the homogeneous layer case, leading to poor values of efficiency away from the resonance. Interestingly, the symmetric case leads to a better conversion efficiency both in reflection (data not shown) and transmission. In fact, this is a direct consequence of the presence of harmonics resonance at wavelengths given by Eq. (9), which may result in mode matching situations where both the pump wavelength and the SHG signal are subject to a resonance. The various scenarii of resonant behaviors in both structures for SHG or DFG are investigated below.

Figure 3 shows the 3 resonant situations that happen in the case of SHG with the respective conversion efficiency spectra. On the one hand, the incoming pump wave at wavelength λ_{pump} can be resonant to increase the quantity of created nonlinear polarization (Fig. 3 (a)). On the other hand, the outgoing signal wave at λ_{SHG} can be resonant to enhance the coupling from the slit to the outer medium (Fig. 3 (b)). When both conditions are fulfilled, it is a mode matching situation (Fig. 3 (c)) where the nonlinear intensity ratio reaches its highest value for a selected period. In the asymmetric resonator, only the cases of Fig. 3 (a) and (b) can happen, thus limiting the value of η to the one obtained when the pump is solely resonant. Using a resonance at the second harmonic wavelength is typically one order of magnitude less efficient, since the energy generated at the second harmonic depends only linearly on the second harmonic electric field (see Eq. 10). In the case of the symmetric resonator, there is always a mode matching situation for SHG between the fundamental resonance at λ and the first order of resonance at $\lambda/2$. The low quality fac-

tors of both resonances can compensate for the natural dispersivity of the material.

There are various configurations of mode matching in both structures for DFG. Two of them are illustrated in the case of the asymmetric (resp. symmetric) resonator in Fig. 4(a) (resp. Fig. 4(b)). In both resonators, there is a degree of freedom to choose the wavelengths in order to be in a two modes matching situation. For instance, the signal wavelength λ_{DFG} determines the geometry of the resonator, and one pump wavelength is chosen so as to match one of the harmonics of the resonator while the last one is determined by the energy conservation condition. The conversion efficiency shown in Fig. 4(a) is comparable to the one obtained for SHG in Fig. 3(a), which is explained by the fact that the pump is degenerate so it could be considered as a degenerate 2 mode matching configuration. Following this previous scheme, three modes matching can be straightforwardly obtained in the symmetric resonator. Indeed, Eq. 9 quantifies the energy of each harmonic wavelength as a multiple of the fundamental wavelength energy. So apart from some peculiar cases, if two of the wavelengths involved in the DFG process have been chosen at resonance wavelengths, the third one is also at another resonance wavelength due to the energy conservation condition (and neglecting the dispersivity). In Fig. 4(b), the fundamental wavelength as well as the two first harmonics wavelengths are used ($\lambda_{\text{pump}}^1 = \lambda_{\text{DFG}}/3$ and $\lambda_{\text{pump}}^2 = \lambda_{\text{DFG}}/2$). As expected, it leads to a higher efficiency conversion ratio than in the two mode matching situation for both transmission and reflection (data not shown). However, this enhancement is lower than for the SHG, due to the fact that the natural dispersivity of the gallium arsenide must be managed for three different wavelengths. To conclude, non lin-

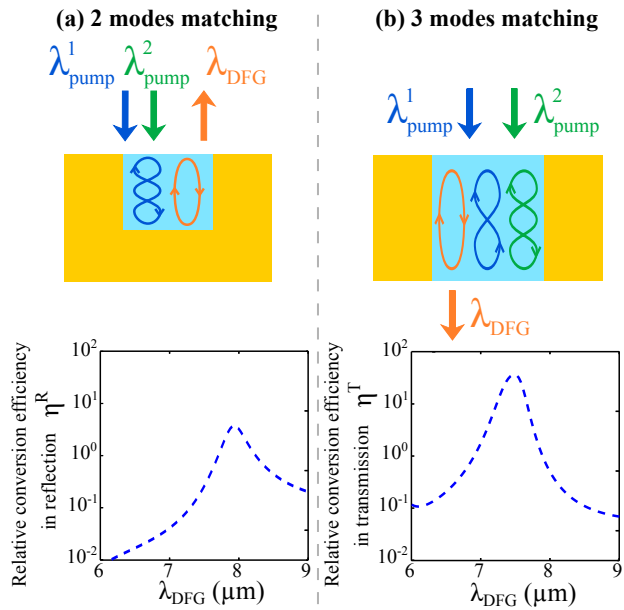


FIG. 4. Two scenarii of modes matching for DFG: (a) two modes matching with one resonant pump and a resonance at the DFG signal in an asymmetric resonator ($h = 0,5 \mu\text{m}$, $h_{\text{GaAs}} = 0,55 \mu\text{m}$), and (b) three modes matching (both resonant pumps and resonant DFG signal) in a symmetric resonator ($h = 1 \mu\text{m}$, $h_{\text{GaAs}} = 1,15 \mu\text{m}$). The efficiency curves are shown below as a function of the pump wavelength. The other parameters are the same in both structures ($d = 1 \mu\text{m}$, $w = 0,2 \mu\text{m}$).

ear phenomena in subwavelength metallic slits or grooves filled with a nonlinear material can be fairly described by this homogenization model. This metamaterial exhibits an unusually high nonlinear effective susceptibility that leads to higher efficiency of the frequency conversion processes, which can be even further enhanced by exploiting mode matching between resonances. It must be emphasized that the metamaterial properties can be spatially tuned, by simply changing the in-plane geometrical parameters, making it possible for instance to address various wavelength ranges. These results can be directly applied to various metals and non linear dielectric materials. In the mid infrared range, the efficiency for thick layer of metamaterials is plagued by the ohmic metallic losses, but it is no longer the case for higher wavelength ranges.

We acknowledge financial support from the ONERA through the MOLIERE project and from a DGA-MRIS scholarship.

* patrick.bouchon@onera.fr

- [1] A. A. Zharov, I. V. Shadrivov, and Y. S. Kivshar, *Physical Review Letters* **91**, 037401 (2003).
 [2] W. Cai, U. K. Chettiar, A. V. Kildishev, and V. M.

- Shalaev, *Nature Photonics* **1**, 224 (2007).
 [3] A. Rose, D. Huang, and D. R. Smith, *Physical Review Letters* **107**, 063902 (2011).
 [4] M. Kauranen and A. V. Zayats, *Nature Photonics* **6**, 737 (2012).
 [5] R. Czaplicki, H. Husu, R. Siikainen, J. Mäkitalo, M. Kauranen, J. Laukkanen, J. Lehtolahti, and M. Kuittinen, *Physical Review Letters* **110**, 093902 (2013).
 [6] M. Lapine, I. V. Shadrivov, and Y. S. Kivshar, *Reviews of Modern Physics* **86**, 1093 (2014).
 [7] J. Lee, M. Tymchenko, C. Argyropoulos, P.-Y. Chen, F. Lu, F. Demmerle, G. Boehm, M.-C. Amann, A. Alù, and M. A. Belkin, *Nature* **511**, 65 (2014).
 [8] A. E. Minovich, A. E. Miroschnichenko, A. Y. Bykov, T. V. Murzina, D. N. Neshev, and Y. S. Kivshar, *Laser & Photonics Reviews* **9**, 195 (2015).
 [9] F. X. Wang, F. J. Rodríguez, W. M. Albers, R. Ahorinta, J. Sipe, and M. Kauranen, *Physical Review B* **80**, 233402 (2009).
 [10] P. Genevet, J.-P. Tetienne, E. Gatzogiannis, R. Blanchard, M. A. Kats, M. O. Scully, and F. Capasso, *Nano Letters* **10**, 4880 (2010).
 [11] K. Thyagarajan, J. Butet, and O. J. Martin, *Nano letters* **13**, 1847 (2013).
 [12] J. E. Sipe and R. W. Boyd, *Phys. Rev. A* **46**, 1614 (1992).
 [13] D. R. Smith and J. B. Pendry, *Journal of the Optical Society of America B* **23**, 391 (2006).
 [14] S. Larouche and D. R. Smith, *Optics Communications* **283**, 1621 (2010).
 [15] S. Park, J. W. Hahn, and J. Y. Lee, *Opt. Express* **20**, 4856 (2012).
 [16] M. Celebrano, X. Wu, M. Baselli, S. Großmann, P. Biagioni, A. Locatelli, C. De Angelis, G. Cerullo, R. Osellame, B. Hecht, L. Duò, F. Ciccacci, and M. Finazzi, *Nature Nanotechnology* **10**, 412 (2015).
 [17] O. Wolf, S. Campione, A. Benz, A. P. Ravikumar, S. Liu, T. S. Luk, E. A. Kadlec, E. A. Shaner, J. F. Klem, M. B. Sinclair, and I. Brener, *Nature Communications* **6** (2015).
 [18] J.-T. Shen, P. B. Catrysse, and S. Fan, *Physical Review Letters* **94**, 197401 (2005).
 [19] D. J. Ironside and J.-T. Shen, *Applied Physics Letters* **102**, 021907 (2013).
 [20] F. Pardo, P. Bouchon, R. Haïdar, and J. Pelouard, *Physical Review Letters* **107**, 93902 (2011).
 [21] P. Bouchon, F. Pardo, B. Portier, L. Ferlazzo, P. Ghenuche, G. Dagher, C. Dupuis, N. Bardou, R. Haïdar, and J. Pelouard, *Applied Physics Letters* **98**, 191109 (2011).
 [22] R. L. Olmon, B. Slovick, T. W. Johnson, D. Shelton, S.-H. Oh, G. D. Boreman, and M. B. Raschke, *Physical Review B* **86**, 235147 (2012).
 [23] T. Skauli, P. Kuo, K. Vodopyanov, T. Pinguet, O. Levi, L. Eyres, J. Harris, M. Fejer, B. Gerard, L. Becouarn, and E. Lallier, *Journal of Applied Physics* **94**, 6447 (2003).
 [24] P. Bouchon, F. Pardo, R. Haïdar, and J. Pelouard, *Journal of the Optical Society of America A* **27**, 696 (2010).
 [25] S. Héron, F. Pardo, P. Bouchon, J.-L. Pelouard, and R. Haïdar, *Journal of the Optical Society of America B* **32**, 275 (2015).
 [26] See Supplemental material at [URL] for Fig. 1 which validates the analytical model of the Metamaterial.